Photoionization of two-electron atoms via the hyperspherical artificial-channel method: Application to H^- and He

Alexander G. Abrashkevich and Moshe Shapiro
Department of Chemical Physics, The Weizmann Institute of Science, 76100, Rehovot, Israel
(Received 23 February 1994)

An application of the artificial-channel method with hyperspherical coordinates to the calculation of photoionization cross sections of two-electron systems is presented. The method yields "bound-free" transition amplitudes and bound-state energies of any two-electron system. It obviates the separate generation of bound- and continuum-state wave functions by calculating directly the desired amplitudes. As applications, the photodetachment cross section of the H^- ion and the photoionization cross section of the He atom have been calculated. The computations are compared with other theoretical calculations and with experiments. The results obtained are in excellent agreement with experimental results for all the energies considered. Of equal significance is the close agreement, attesting to the high accuracy of the method, between results obtained by using the length form for the field-matter interaction and those obtained with the acceleration form.

PACS number(s): 32.80.Fb, 31.50.+w, 32.70.Cs, 32.80.Dz

I. INTRODUCTION

Photoionization of two-electron systems is a subject of growing interest, as it sheds light on the role of electronic correlations in both bound and continuum states. When a number of channels are open, photoionization processes result in a rich spectrum of doubly excited highly correlated autoionizing states. Such resonances were observed recently for He [1,2] and the H^- ion [3,4]. These observations are complemented by new measurements of field-induced window-type resonances in electron detachment of H^- in the static electric field ($F \leq 90$ kV/cm) [5,6], leading to the production of ($N=4$, 5, and 6) neutral H atoms.

The study of doubly excited atoms poses a number of interesting challenges, as we need to properly describe the dynamics induced by several interacting continua and we need to account for strong correlational effects. Configuration interaction by basis-set expansion methods becomes very cumbersome for treating doubly excited resonances because of the vast number of configurations needed to account for the strong electronic correlation existing for these states. The problem becomes even more severe when the system does not have atomic symmetry. Because of this, a variety of specialized procedures have been employed [7–18]. These procedures include R-matrix methods [8,9], coupled-integral equations within many-body perturbation theory [10], multiconfigurational Hartree-Fock [11,12], continuum discretization methods [13–15], the complex Kohn variational method [16], and hyperspherical close-coupling schemes [17,18].

All the above methods go through two phases in which the continuum and bound wave functions are first obtained; the "bound-free" transition dipole matrix elements are computed from these wave functions by numerical integration. This procedure is costly and fraught with inaccuracies because of two main reasons: (a) At sufficiently high energies the continuum wave functions are highly oscillatory. They therefore need to be generated and stored at many points. (b) If one uses propagation techniques, the generation of the continuum wave function necessitates the continual applications of stabilizing transformations in order to get rid of the exponentially growing components of the closed channels. These stabilizing transformations must be undone after the propagation is finished in order to obtain the wave functions. The undoing of the stabilizing transformation is time consuming and is a source of errors. In fact, the errors propagate exponentially with the number of steps at which the stabilizing transformation is undone.

In this paper we present a method, an application of the artificial channel method (ACM) [19,20], which overcomes the above-mentioned difficulties. We present an application to photoionization processes of the artificial channel method, which has so far been applied to nuclear-type problems (e.g., photodissociation [19–21]). The main merit of the method is that it does not require the explicit generation and storage of continuum or bound wave functions. Rather, the relevant bound-free matrix elements (and the bound-state energies) are computed from a single set of equations. An additional benefit is that, because of the above, it is possible to use algorithms, such as the log-derivative or piecewise-analytic methods [22,23], which take steps larger than those necessary for convergence of the bound-free integral by ordinary quadrature. Moreover, since the bound and continuum wave functions are treated on an equal footing, they are of identical accuracy, a point of great importance to the overall accuracy of the bound-free integrals. A drawback of the method is that because both bound and continuum spaces are included in a single set of equations its size is larger than that of the separate spaces. This drawback is more than offset by the ease of computation, the great stability of the method, and the ability to take much larger propagation

steps.

For the case of two-electron systems we found it useful to use the hyperspherical coordinates [24–26] which allow for the description of exchange symmetry in these systems in a very natural way. In the hyperspherical coordinates the motion of the electrons in $\mathbb{R}^6$ space is separated into the S^5 angular variables [27] and the "hyper-radius" $\rho=\sqrt{r_1^2+r_2^2}$, which acts as the scattering coordinate. The goodness of the hyperspherical method derives from the success of the hyperspherical adiabatic (HSA) approximation [26–36]. The expansion in the HSA basis was performed for the photoionization of He [18], and for the doubly excited states [17,34–37] in particular.

This paper is organized as follows: In Sec. II we outline the hyperspherical artificial channel method. In Sec. III we present the results for the He and H^- bound states, the photoionization of He, and photodetachment of H^-. Future applications are discussed in the Conclusions section.

II. METHOD

A. Photoionization cross section

In the weak-field limit, the cross section for photoionization or photodetachment of an atom by a single photon is given in the length form by

$$\sigma_L(\omega)=4\pi^2\omega\alpha|f_L|^2 , \tag{1}$$

and in the acceleration form by

$$\sigma_A(\omega)=\frac{4\pi^2\alpha}{\omega^3}|f_A|^2 , \tag{2}$$

where

$$f_L(\omega)=\left\langle \Psi_E^- \left| \hat{\boldsymbol{\varepsilon}}\cdot\sum_{i=1}^{2}\mathbf{r}_i \right| \Psi_n \right\rangle \tag{3}$$

and

$$f_A(\omega)=\left\langle \Psi_E^- \left| \hat{\boldsymbol{\varepsilon}}\cdot\sum_{i=1}^{2}\frac{Z\mathbf{r}_i}{r_i^3} \right| \Psi_n \right\rangle \tag{4}$$

are, respectively, the length- and acceleration-form transition amplitudes. The wave functions Ψ_n and Ψ_E^- represent, respectively, the bound and the continuum states; ω is the photon energy in atomic units, α is a fine-structure constant, Z is a nuclear charge, $\hat{\boldsymbol{\varepsilon}}$ is the field's polarization direction, and $\mathbf{r}_i$ is the radius vector of the ith electron. When the bound and continuum wave functions are exact, the length and acceleration forms should yield identical results in the weak-field limit.

B. Hyperspherical coordinates

The Schrödinger equation for a two-electron atom is given by

$$\left\{\sum_{i=1}^{2}\left[-\frac{\Delta_i}{2}-\frac{Z}{r_i}\right]+\frac{1}{|\mathbf{r}_1-\mathbf{r}_2|}-E\right\}\psi(\mathbf{r}_1,\mathbf{r}_2)=0 , \tag{5}$$

where Δ_i is Laplacian for the ith electron. In hyperspherical coordinates r_1 and r_2 are replaced by the hyper-radius ρ and hyperangle α defined by

$$\rho=\sqrt{r_1^2+r_2^2} , \quad \alpha=\tan^{-1}(r_2/r_1) . \tag{6}$$

Expressed in these coordinates, the Schrödinger equation for the "hyperspherical" wave function $\Psi(\rho,\Omega)\equiv(\rho^{5/2}\sin\alpha\cos\alpha)\psi$ has the following form:

$$\left[-\frac{\partial^2}{\partial\rho^2}-\frac{1}{4\rho^2}+\hat{h}(\rho)-2E\right]\Psi(\rho,\Omega)=0 , \tag{7}$$

where

$$\hat{h}(\rho)=\frac{1}{\rho^2}\hat{\Lambda}^2(\Omega)+\frac{1}{\rho}V(\alpha,\theta_{12}) , \tag{8}$$

$$\hat{\Lambda}^2(\Omega)=-\frac{\partial^2}{\partial\alpha^2}+\frac{l_1^2}{\cos^2\alpha}+\frac{l_2^2}{\sin^2\alpha} , \tag{9}$$

and

$$V(\alpha,\theta_{12})=-\frac{2Z}{\cos\alpha}-\frac{2Z}{\sin\alpha}+\frac{2}{\sqrt{1-\sin2\alpha\cos\theta_{12}}} . \tag{10}$$

Here Ω represent the five angles $\alpha,\hat{\mathbf{r}}_1,\hat{\mathbf{r}}_2$; l_i is the orbital angular momentum of the ith electron, and $\theta_{12}=\cos^{-1}[(\mathbf{r}_1\cdot\mathbf{r}_2)/r_1r_2]$.

C. Hyperspherical adiabatic (HSA) basis

The HSA states $\{\Phi_\mu(\Omega;\rho)\}$ are defined as the solutions of the eigenvalue equation,

$$\hat{h}(\rho)\Phi_\mu(\Omega;\rho)=U_\mu(\rho)\Phi_\mu(\Omega;\rho) . \tag{11}$$

Equation (11) must be solved for each ρ value to obtain the hyperspherical potential $U_\mu(\rho)$. For large values of ρ the HSA functions take on the character of the hydrogenic wave functions perturbed by a distant charged particle. For ρ close to the origin the HSA states resemble the hyperspherical harmonics (K harmonics [26]), defined as the eigenfunctions of $\hat{\Lambda}^2(\Omega)$, the generalized angular momentum operator.

Following Ref. [38], we solve Eq. (11) by expanding $\Phi_\mu(\Omega;\rho)$ in a ρ-changing basis of Ω-dependent functions,

$$\Phi_\mu(\Omega;\rho)=\sum_{\substack{l_1l_2k\\ l_1\le l_2}} a^\mu_{l_1l_2k}(\rho)\Theta^{LMS\pi}_{l_1l_2k}(\Omega;\rho) , \tag{12}$$

where

$$\Theta^{LMS\pi}_{l_1l_2k}(\Omega;\rho)=\frac{1}{\sqrt{2}}[\mathcal{Y}^{LM}_{l_1l_2}(\hat{\mathbf{r}}_1,\hat{\mathbf{r}}_2)g_k^{l_1l_2}(\alpha;\rho)+(-1)^{L+S+l_1+l_2}\mathcal{Y}^{LM}_{l_2l_1}(\hat{\mathbf{r}}_1,\hat{\mathbf{r}}_2)g_k^{l_1l_2}(\pi/2-\alpha;\rho)] \text{ for } l_1\neq l_2 , \tag{13}$$

$$\Theta^{LMS\pi}_{llk}(\Omega;\rho)=\mathcal{Y}^{LM}_{ll}(\hat{\mathbf{r}}_1,\hat{\mathbf{r}}_2)g_k^{ll}(\alpha;\rho) \text{ for } l_1=l_2=l , \tag{14}$$

with $\mathcal{Y}^{LM}_{l_1 l_2}(\hat{\mathbf{r}}_1,\hat{\mathbf{r}}_2)$ being the bipolar spherical harmonics. The quantum numbers L, M, S, and π are, respectively, the total angular momentum, its projection onto the z axis, the total spin, and total parity. The $g_k^{l_1 l_2}(\alpha;\rho)$ functions are chosen as the solutions of the following eigenvalue equation:

$$\left\{\frac{1}{\rho^2}\left[-\frac{\partial^2}{\partial\alpha^2}+\frac{l_1(l_1+1)}{\cos^2\alpha}+\frac{l_2(l_2+1)}{\sin^2\alpha}\right]+\frac{1}{\rho}\langle\mathcal{Y}^{LM}_{l_1 l_2}|V(\alpha,\theta_{12})|\mathcal{Y}^{LM}_{l_1 l_2}\rangle\right\}g_k^{l_1 l_2}(\alpha;\rho)=\epsilon_k^{l_1 l_2}(\rho)g_k^{l_1 l_2}(\alpha;\rho) \tag{15}$$

subject to the boundary conditions,

$$g_k^{l_1 l_2}(\alpha=0;\rho)=g_k^{l_1 l_2}(\alpha=\pi/2;\rho)=0\ . \tag{16}$$

Substitution of the expansion of Eq. (12) into Eq. (11) leads to a set of algebraic eigenvalue equations for the $a^{\mu}_{l_1 l_2 k}(\rho)$ coefficients,

$$\mathbf{h}\mathbf{a}=\mathbf{a}\hat{\mathbf{U}}\ , \tag{17}$$

where

$$\hat{\mathbf{U}}_{\mu,\mu'}=U_{\mu}(\rho)\delta_{\mu,\mu'}\ , \tag{18}$$

$$\mathbf{a}^T=(a_1,a_2,\ldots,a_n)\ ,\quad a_i=a^{\mu}_{l_1 l_2 k}(\rho)\ ,\quad i=1,2,\ldots,n, \tag{19}$$

and

$$h^{l_1' l_2' k'}_{l_1 l_2 k}(\rho)=\langle\Theta^{LMS\pi}_{l_1 l_2 k}(\Omega;\rho)|\hat{h}(\rho)|\Theta^{LMS\pi}_{l_1' l_2' k'}(\Omega;\rho)\rangle\ . \tag{20}$$

Since $\mathbf{h}$ is a real symmetric matrix, Eq. (17) can be easily solved by standard diagonalization methods.

We obtain the solutions of Eqs. (15) and (16) by a finite-element method [39] with isoparametric Lagrange elements of the nth order. The method is accurate to $O(h_\alpha^{2n})$ with respect to the $\epsilon_k^{l_1 l_2}(\rho)$ eigenvalues and to $O(h_\alpha^{n+1})$ with respect to the $g_k^{l_1 l_2}(\alpha;\rho)$ eigenfunctions, where h_α is the length of one of the $N_{\rm el}$ grid elements of order $n=N_{\rm pol}$ spanning the $[0,\pi/2]$ interval. The resulting generalized eigenvalue problem is solved by the subspace iteration method [39].

The numerical integrations of the $\langle\mathcal{Y}^{LM}_{l_1 l_2}|V(\alpha,\theta_{12})|\mathcal{Y}^{LM}_{l_1 l_2}\rangle$ angular matrix elements and the transition-dipole angular matrix elements are carried out with a 450-node Gauss-Legendre quadrature. Numerical parameters, such as $N_{\rm el}$, $N_{\rm pol}$, the maximal value of l_1, l_2, and k of Eq. (12), are adjusted to render $U_\mu(\rho)$ and $\Phi_\mu(\Omega;\rho)$ accurate to 10^{-4}–10^{-5} a.u. Representative values of these numerical parameters are given in Table I.

As reported below, the HSA expansion converges well, with the rate of convergence improving as ρ increases. This trend is probably due [38] to the $\Theta^{LMS\pi}_{l_1 l_2 k}(\Omega;\rho)$ functions accounting for the main part of the interaction. This is in sharp contrast to the hyperspherical harmonics method [26] where the rate of convergence *decreases* as ρ increases.

In Figs. 1(a)–1(c) we present the H^- $^1S^e$ and $^1P^o$ and the He $^1P^o$ potential curves correlating with the $n=1$–$n=5$ hydrogeniclike states as a function of ρ. Clearly seen are points of avoided crossings [26] where the radial nonadiabatic coupling terms are known [26,34,36] to peak. If these peaks are very sharp, the use of the adiabatic basis may be problematic. In this case it is advisable to switch to some *diabatic* representation [40,41] (i.e., a representation in which the first-derivative coupling terms vanish). One convenient type of diabatic basis is the so-called sector-diabatic basis [38,42] which satisfies Eq. (17) in the middle of each ρ sector only. Propagation with this basis necessitates transforming from one sector basis to another, as one moves across the sectors, in order to guarantee the continuity of the total wave function $\Psi(\rho,\Omega)$. As described below, this is in fact the procedure adopted here.

D. Coupled-channel expansion

With the introduction of the HSA expansion, the six-dimensional Schrödinger equation [Eq. (7)] is transformed to a system of coupled differential equations ("coupled channels") in ρ. In the sector-diabatic method we divide the range of ρ values into $[\rho_{q-1},\rho_q]$, $q=1,\ldots,N$ sectors and use in each sector a diabatic basis obtained by solving Eq. (17) at the $\bar{\rho}_q=(\rho_{q-1}+\rho_q)/2$, $q=1,\ldots,N$ midpoints.

In principle, the sector-diabatic basis is used to expand both the bound, $\Psi_n(\rho,\Omega)$, and continuum, $\Psi^-_E(\rho,\Omega)$ wave functions,

$$\Psi_n(\rho,\Omega)=\sum_\mu B_\mu(\rho;\bar{\rho}_q)\Phi^B_\mu(\Omega;\bar{\rho}_q)\ , \tag{21}$$

$$\Psi^-_E(\rho,\Omega)=\sum_\mu C^-_\mu(E|\rho;\bar{\rho}_q)\Phi^C_\mu(\Omega;\bar{\rho}_q)\ . \tag{22}$$

TABLE I. Numerical parameters used for calculating the HSA eigenvalue curves and corresponding basis functions. Below $\mu_{\max}$ is the number of basis functions $\Phi_\mu(\Omega;\rho)$, $l_{\max}$ is the maximal value of orbital momentum l for all pairs (l_1,l_2) allowed, $k_{\max}$ is the number of solutions of Eq. (15), $N_{\rm el}$ is the number of finite elements, $N_{\rm pol}$ is the order of isoparametric Lagrange elements used as the finite element shape functions, and h_α is a typical step of the finite element grid.

Numerical scheme parameters	H^-		He	
	$^1S^e$	$^1P^o$	$^1S^e$	$^1P^o$
$\mu_{\max}$	15	25	15	25
$l_{\max}$	8	5	9	5
$k_{\max}$	9	10	10	11
$N_{\rm el}$	172	200	160	188
$N_{\rm pol}$	4	4	5	5
h_α	0.0091	0.0079	0.0098	0.0084

$B_\mu(\rho;\bar{\rho}_q)$ and $C_\mu^-(E|\rho;\bar{\rho}_q)$, the "channel wave functions" in the bound and continuum manifolds, satisfy similar sets of coupled-channel equations,

$$\left\{-\frac{d^2}{d\rho^2}\mathbf{I}+\mathbf{V}^B(\rho)-2E_n\mathbf{I}\right\}\mathbf{B}_n(\rho;\bar{\rho}_q)=0\ , \tag{23a}$$

$$\left\{-\frac{d^2}{d\rho^2}\mathbf{I}+\mathbf{V}^C(\rho)-2E\mathbf{I}\right\}\mathbf{C}^-(E|\rho;\bar{\rho}_q)=0\ , \tag{23b}$$

differing only in the boundary conditions and the numerical values of the potential matrix elements,

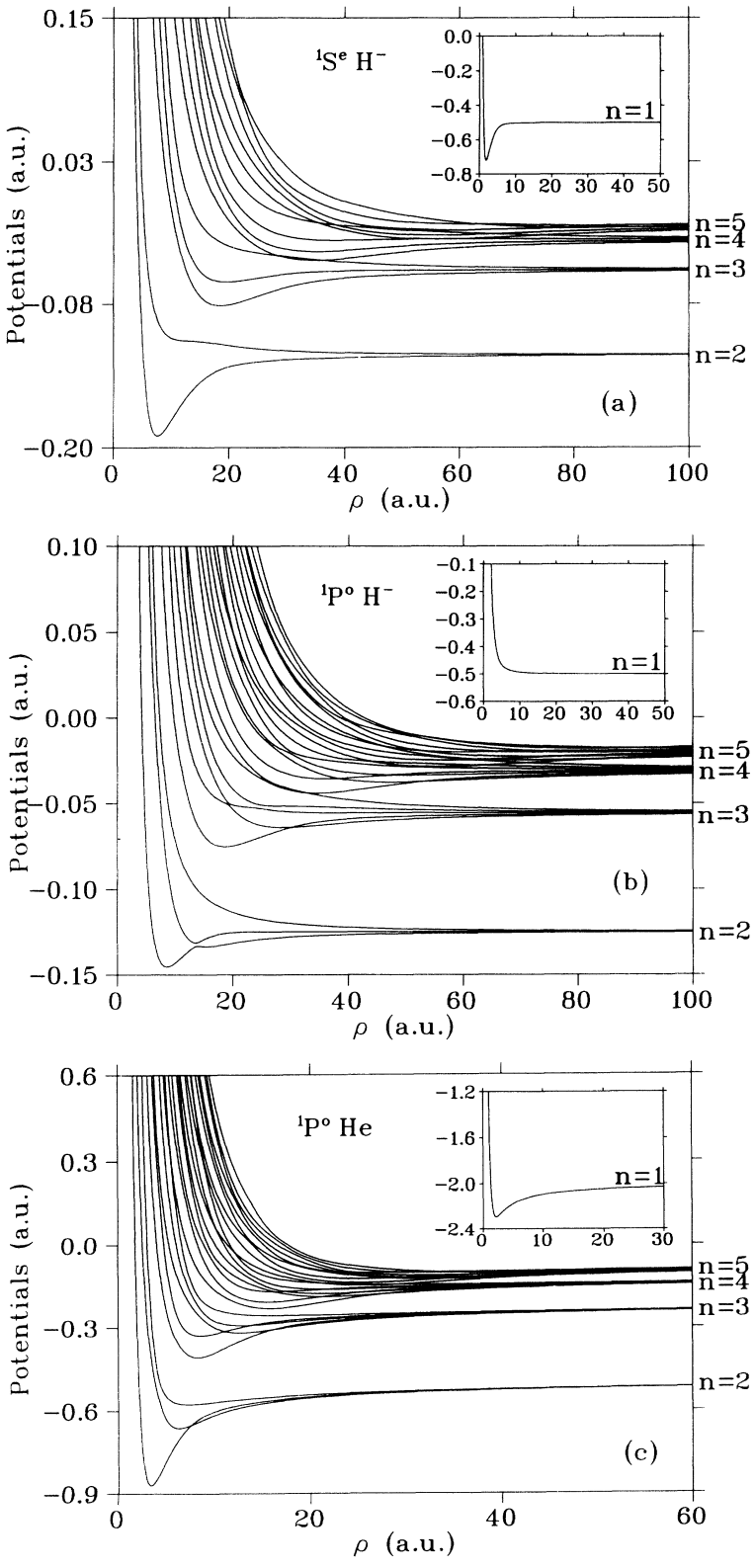

FIG. 1. Potential curves $U_\mu(\rho)$ (in a.u.) plotted vs hyper-radius ρ up to the $n=5$ threshold for (a) $^1S^e$ state of H^-; (b) $^1P^o$ state of H^-; (c) $^1P^o$ state of He.

$$V^{\sigma}_{\mu\nu}(\rho)=-\frac{1}{4\rho^2}\delta_{\mu\nu}+\left[\frac{\bar{\rho}_q}{\rho}\right]^2 U^{\sigma}_{\mu}(\bar{\rho}_q)\delta_{\mu\nu} +2\left[\frac{1}{\rho}-\frac{\bar{\rho}_q}{\rho^2}\right] \times\langle\Phi^{\sigma}_{\mu}(\Omega;\bar{\rho}_q)|V(\alpha,\theta_{12})|\Phi^{\sigma}_{\nu}(\Omega;\bar{\rho}_q)\rangle\ , \quad \sigma=B,C\ . \tag{24}$$

In practice we solve for a single set of equations, as discussed below.

The change from one sector to the next must maintain the continuity of the $\Psi^{-}_{E}(\rho,\Omega)$ wave function and its derivative at the sector borders. This is accomplished by expressing the channel wave functions on the left-hand side (lhs) of the $n+1$ sector in terms of the channel wave functions on the right-hand side (rhs) of the nth sector. Using the identity between the total wave functions at the border point,

$$\sum_{\mu} C_{\mu}(\rho_R;\bar{\rho}_n)\Phi^{C}_{\mu}(\Omega;\bar{\rho}_n)=\sum_{\mu} C_{\mu}(\rho_L;\bar{\rho}_{n+1})\Phi^{C}_{\mu}(\Omega;\bar{\rho}_{n+1})\ , \tag{25}$$

we obtain

$$C_{\mu}(\rho_L;\bar{\rho}_{n+1})=\sum_{\nu} Q^{n}_{\mu,\nu}C_{\nu}(\rho_R;\bar{\rho}_n)\ , \tag{25a}$$

where the sector overlap matrix $\mathbf{Q}^n$ is defined as

$$Q^{n}_{\mu,\nu}=\langle\Phi^{C}_{\mu}(\Omega;\bar{\rho}_{n+1})|\Phi^{C}_{\nu}(\Omega;\bar{\rho}_n)\rangle\ . \tag{25b}$$

The bound-state equations may be treated in an identical manner. A good check of the accuracy of the basis functions and the sector size is the unitarity of $\mathbf{Q}^n$ overlap matrices. We have found that a uniform width of $0.2a_0$ guarantees the unitarity of the overlap matrices to within 10^{-3}–10^{-4} over the entire $\rho\in[0.1,125.]$ range used in our computations.

E. Dipole matrix elements

The dipole transition amplitudes are obtained by substitution of Eqs. (21) and (22) into Eqs. (3) and (4),

$$f_L(\omega)=\sum_{\mu\nu}\langle C^{-}_{\mu}(E)|d^{L}_{\mu\nu}(\rho)|B_{\nu}\rangle\ , \tag{26}$$

$$f_A(\omega)=\sum_{\mu\nu}\langle C^{-}_{\mu}(E)|d^{A}_{\mu\nu}(\rho)|B_{\nu}\rangle\ , \tag{27}$$

where $d^{L(A)}_{\mu\nu}(\rho)$, the angular dipole matrix elements, are given as

$$d^{L}_{\mu\nu}(\rho)=\rho D^{L}_{\mu\nu}(\bar{\rho}_q)\ , \tag{28}$$

$$d^{A}_{\mu\nu}(\rho)=\frac{Z}{\rho^2}D^{A}_{\mu\nu}(\bar{\rho}_q)\ . \tag{29}$$

$D^{L}_{\mu\nu}(\bar{\rho}_q)$ and $D^{A}_{\mu\nu}(\bar{\rho}_q)$ are given as [29]

$$D^{L}_{\mu\nu}(\bar{\rho}_q)=\langle\Phi^{C}_{\mu}(\Omega;\bar{\rho}_q)|(\cos\alpha\cos\theta_1+\sin\alpha\cos\theta_2)|\Phi^{B}_{\nu}(\Omega;\bar{\rho}_q)\rangle\ , \tag{30}$$

$$D^{A}_{\mu\nu}(\bar{\rho}_q)=\left\langle\Phi^{C}_{\mu}(\Omega;\bar{\rho}_q)\left|\left[\frac{\cos\theta_1}{\cos^2\alpha}+\frac{\cos\theta_2}{\sin^2\alpha}\right]\right|\Phi^{B}_{\nu}(\Omega;\bar{\rho}_q)\right\rangle\ . \tag{31}$$

The $D_{\mu\nu}$ matrix elements are independent of the final-state energy E and are the same for any photon energy ω. In Figs. 2 and 3 we show the radial dependence of $D_{\mu\nu}$ for the ^1S-^1P transition in H^- and He. These matrix elements approach a constant value as ρ tends to infinity. Near the origin they depend strongly on ρ (except for the diagonal elements in the length form) as a result of electronic correlations. In general, the variance with ρ of the acceleration-form matrix elements exceeds that of the length form. The nondiagonal matrix elements quickly decrease with the number of channels μ and with ρ. As can be seen in Figs. 2 and 3 the behavior of the angular dipole matrix elements in the vicinity of the avoided-crossing points, occurring at 13.66 a.u. for the $^1P^o$ state of H^- and at 7.65 and 17.43 a.u. for the $^1P^o$ state of He (see Fig. 1), is rather erratic. This is as expected due to the rapid change in the HSA basis near the crossing points. Again, the problem is resolved in the sector-diabatic representation used here.

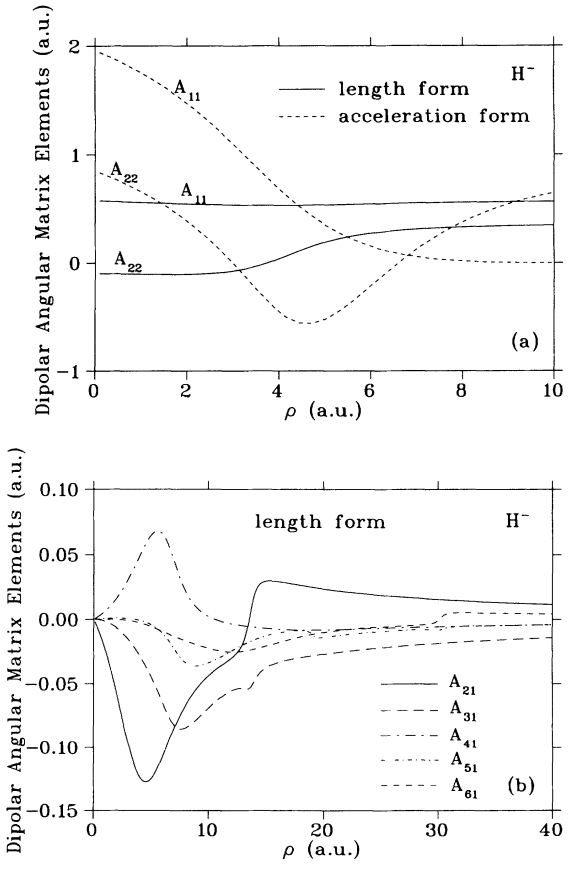

FIG. 2. Radial dependence of the angular matrix elements $D_{\mu\nu}$ in the length and acceleration forms for ^1S-^1P transition in H^-. (a) $\mu=\nu=1,2$; (b) $\mu=1,2,\ldots,6$, $\nu=1$.

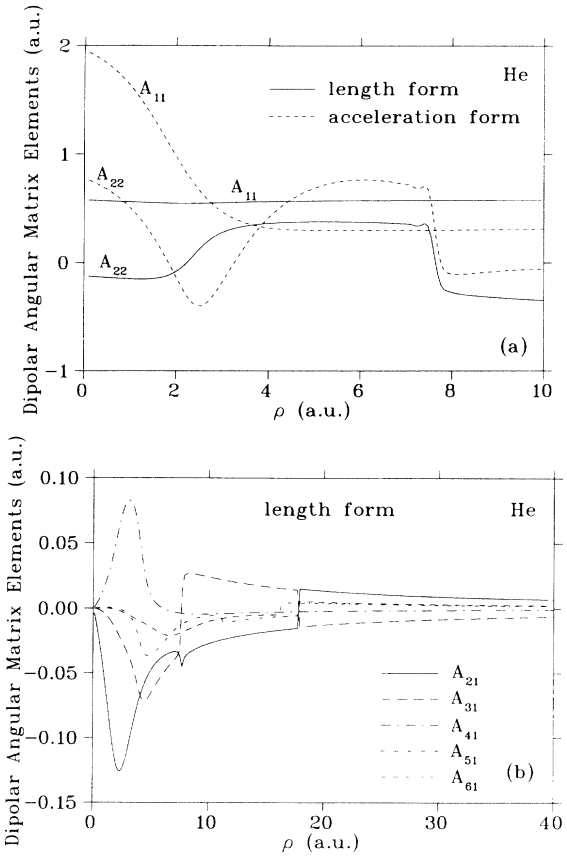

FIG. 3. Radial dependence of the angular matrix elements $D_{\mu\nu}$ in the length and acceleration forms for ^1S-^1P transition in He. (a) $\mu=\nu=1,2$; (b) $\mu=1,2,\ldots,6$, $\nu=1$.

F. Artificial-channel method

In the artificial-channel method one solves a single set of coupled-channel equations for the bound and continuum manifolds. An additional ("artificial") channel, serving as a source term, is introduced in order to satisfy the incompatible boundary conditions imposed on these two manifolds. In the hyperspherical sector-diabatic representation the artificial-channel set of equations is composed of the following:

A continuum manifold,

$$\left[-\frac{d^2}{d\rho^2}-E\right]F_\mu^C(\rho;\bar{\rho}_q)+\sum_\nu V_{\mu\nu}^C(\rho)F_\nu^C(\rho;\bar{\rho}_q) = \sum_\nu d_{\mu\nu}(\rho)F_\nu^B(\rho;\bar{\rho}_q)\ , \quad (32)$$

coupled to a bound manifold,

$$\left[-\frac{d^2}{d\rho^2}-E\right]F_\mu^B(\rho;\bar{\rho}_q)+\sum_\nu V_{\mu\nu}^B(\rho)F_\nu^B(\rho;\bar{\rho}_q) = W_\mu(\rho)F^a(\rho;\bar{\rho}_q)\ , \quad (33)$$

coupled to the artificial channel,

$$\left[-\frac{d^2}{d\rho^2}-E+\epsilon_a+V^a(\rho)\right]F^a(\rho;\bar{\rho}_q)=0\ , \quad (34)$$

which serves as the source term. The $V_{\mu\nu}^C(\rho)$ and $V_{\mu\nu}^B(\rho)$ matrices in the above are given by Eq. (24), ϵ_a is the artificial-channel asymptotic energy, and the dipole matrix elements $d_{\mu\nu}(\rho)$ are given by Eqs. (28) and (29). As explained below, the results for the final bound-free matrix elements are insensitive to the exact form of $V^a(\rho)$ and $W_\mu(\rho)$ of the above. In the present application [43] both are taken to be simple decaying exponentials $V_0\exp(-a\rho)$.

Equations (32)–(34) can be written more compactly in matrix notation as

$$\left\{\left[-\frac{d^2}{d\rho^2}-E\right]\mathbf{I}+\mathbf{V}(\rho)\right\}\mathbf{F}(\rho)=0\ , \quad (35)$$

where the potential matrix is of the form

$$\mathbf{V}(\rho)=\begin{bmatrix} V^a(\rho)+\epsilon^a & \mathbf{0}^\dagger & 0^\dagger \\ 0 & \mathbf{V}^C(\rho) & \mathbf{d}(\rho) \\ W(\rho) & 0 & \mathbf{V}^B(\rho) \end{bmatrix}\ . \quad (36)$$

The matrix of solutions is of the form

$$\mathbf{F}(\rho)=\begin{bmatrix} F_a^a & 0^\dagger & 0^\dagger \\ F_C^a & \mathbf{F}_C^C & \mathbf{F}_C^B \\ F_B^a & \mathbf{F}_B^C & \mathbf{F}_B^B \end{bmatrix}\ . \quad (37)$$

In the above, boldface symbols represent rectangular submatrices, italic symbols represent column vectors, and † represents a Hermitian adjoint (for real matrices, a matrix transpose). For example 0, 0, and $0^\dagger$ denote zero rectangular matrix, zero column vector, and zero row vector, respectively.

The **S** matrix derived from Eq. (35) can be obtained using a variety of multichannel propagation schemes [22]. Of greatest interest to us are the elements of the **S** matrix that connect the artificial channel to the continuum subspace. These matrix elements can be written, using standard expressions, as

$$S_{C,a}(E)=2\pi i\langle\mathbf{C}^-(E)|d|F_B^{+a}(E)\rangle\ , \quad (38)$$

with $\langle\mathbf{C}^-(E)|$ being the (incoming) solutions within the continuum manifold [Eq. (23b)]. It can be shown [19,20] that with the special nonsymmetric form of Eq. (35) the above matrix elements become

$$S_{C,a}(E)=2\pi i\sum_n\frac{\langle\mathbf{C}^-(E)|d|B_n\rangle\langle B_n^\dagger|W|F_a^{a+}(E)\rangle}{E-E_n}\ , \quad (39)$$

where E_n are the eigenenergies and B_n are the columns of eigenstate coefficients in the bound manifold [Eq. (23a)].

It follows from Eq. (39) that all the elements belonging to the $S_{C,a}$ column have poles at E_n—the bound-state energies of the (two-electron) system. The *residues* of these poles are directly related to the desired dipole transition amplitudes

$$f_{\mu,n}(E)\equiv\langle C^{-\mu}(E)|d|B_n\rangle=\frac{1}{2\pi i}\mathrm{Res}_n\left\{\frac{S_{\mu,a}(E)}{w^n(E)}\right\}, \quad (40)$$

where

$$w^n(E)=\langle B_n^\dagger|W|F_a^{+a}(E)\rangle . \quad (41)$$

The quantity w^n and the bound-state energies E_n are most conveniently calculated in a separate smaller calculation in which the whole **C** manifold is replaced by a second artificial channel a' whose $V^{a'}$ channel potential and $W^\dagger$ row vector of coupling terms (like **C**, channel a' is coupled to the bound manifold) are set identical to V^a and W. The $S_{a',a}$ matrix element resulting from this set of equations, which is identical in structure to Eq. (35), is of the form

$$S_{a',a}(E)=2\pi i\sum_n\frac{\langle F_{a'}^{a'-}(E)|W^\dagger|B_n\rangle\langle B_n^\dagger|W|F_a^{a+}(E)\rangle}{E-E_n}$$

$$=2\pi i\exp(2i\delta_a)\sum_n|w^n(E)|^2/(E-E_n) . \quad (42)$$

Hence $|w^n(E_n)|^2$ are obtained as

$$|w^n(E_n)|^2=\left|\frac{1}{2\pi}\mathrm{Res}_n S_{a',a}(E)\right| , \quad (43)$$

and E_n are obtained as the corresponding poles positions. These poles can be located very efficiently [44] using only a few iterations. (See Appendix A of Ref. [44].) Typically [45] an eigenvalue can be located to nine to ten significant figures with four or five evaluations of the **S**-matrix element. Once $w^n(E_n)$ and E_n are known, the desired bound-free matrix elements are computed directly from Eq. (39). A simple shift of $E-E_n$ in the definition of the ϵ_a asymptotic energy guarantees that it is enough to solve Eq. (43) only once, i.e., that the value of $w^n(E_n)$ may be used for all energies [19].

Finally, we outline our procedure for extracting the **S**-matrix elements. As mentioned above the propagation of Eq. (35) is performed with the log-derivative method [22]. In the asymptotic region we must transform the solutions from the hyperspherical coordinates to the heliocentric $(\mathbf{r}_1,\mathbf{r}_2)$ coordinate system, in terms of which the asymptotic form of the two-electron wave function is

$$\Psi_i(\mathbf{r}_1,\mathbf{r}_2)=\sum_j\phi_j(r_2,\hat{\mathbf{r}}_1,\hat{\mathbf{r}}_2)\chi_{ji}^E(k_jr_1)$$

$$=\sum_j\phi_j(r_2,\hat{\mathbf{r}}_1,\hat{\mathbf{r}}_2)\times\{k_j^{-1/2}j_{l_j}(k_jr_1)\delta_{ji}+k_j^{-1/2}n_{l_j}(k_jr_1)K_{ji}\} , \quad (44)$$

where

$$\phi_j(r_2,\hat{\mathbf{r}}_1,\hat{\mathbf{r}}_2)=P_{nl_2}(r_2)\mathcal{Y}_{l_1l_2}^{LM}(\hat{\mathbf{r}}_1,\hat{\mathbf{r}}_2) , \quad j\equiv(n,l_1,l_2) , \quad (45)$$

with $P_{nl_2}(r_2)$ being the radial hydrogenic wave functions. k_n is the channel wave number given by

$$k_n=\sqrt{2(E-\epsilon_n)} , \quad \epsilon_n=-Z^2/2n^2 , \quad (46)$$

K_{ij} are the elements of the reactance K matrix, and $j_{l_j}(k_jr_1)$ and $n_{l_j}(k_jr_1)$ are spherical Riccati-Bessel and Riccati-Neumann functions, respectively. Equating Eqs. (22) and (44), and using the orthonormality of the basis functions $\Phi_\mu(\Omega;\rho_{as})$, we have

$$F_{\mu i}(\rho_{\mathrm{as}})=\sum_j\{\mathcal{J}_{\mu j}(\rho_{\mathrm{as}})\delta_{ji}+\mathcal{G}_{\mu j}(\rho_{\mathrm{as}})K_{ji}\} , \quad (47)$$

where

$$\mathcal{J}_{\mu j}(\rho_{\mathrm{as}})=N\left[\frac{\rho_{\mathrm{as}}}{k_n}\right]^{1/2}\sum_k a_{l_1l_2k}^{\mu}(\rho_{\mathrm{as}})\int_0^{\pi/2}d\alpha\, g_k^{l_1l_2}(\alpha;\rho_{\mathrm{as}})P_{nl_2}(\rho_{\mathrm{as}}\sin\alpha)j_{l_j}(k_n\rho_{\mathrm{as}}\cos\alpha) , \quad (48)$$

$$\mathcal{G}_{\mu j}(\rho_{\mathrm{as}})=N\left[\frac{\rho_{\mathrm{as}}}{k_n}\right]^{1/2}\sum_k a_{l_1l_2k}^{\mu}(\rho_{\mathrm{as}})\int_0^{\pi/2}d\alpha\, g_k^{l_1l_2}(\alpha;\rho_{\mathrm{as}})P_{nl_2}(\rho_{\mathrm{as}}\sin\alpha)n_{l_j}(k_n\rho_{\mathrm{as}}\cos\alpha) , \quad (49)$$

with N being a normalization constant, $N=1$ for $l_1=l_2$ and $N=1/\sqrt{2}$ for $l_1\neq l_2$. ρ_{as} is the end point of the integration region in variable ρ. Equation (47) can be written in matrix notations as

$$\mathbf{F}=\mathcal{J}+\mathcal{G}\mathbf{K} . \quad (50)$$

Matching the log-derivative matrix in hyperspherical coordinates to the transformed asymptotic form on the $\rho=\rho_{\mathrm{as}}$ hypersphere gives

$$\mathbf{Z}=(\mathcal{J}'+\mathcal{G}'\mathbf{K})(\mathcal{J}+\mathcal{G}\mathbf{K})^{-1} , \quad (51)$$

where prime denotes differentiation with respect to ρ. Partitioning the matrices into open-open, open-closed, closed-open, and closed-closed submatrices leads to the following equation for the open-open portion of the **K** matrix:

$$(\mathbf{Z}\mathcal{G}-\mathcal{G}')_{oo}\mathbf{K}_{oo}=(\mathcal{J}'-\mathbf{Z}\mathcal{J})_{oo} . \quad (52)$$

To extract the open-channel K matrix we need only $\mathcal{J}_{oo}$, $\mathcal{G}_{oo}$, $\mathcal{J}_{co}$, and $\mathcal{G}_{co}$ submatrices, so Eq. (52) can be reduced to

$$(\mathbf{Z}_{oc}\mathcal{G}_{co}-\mathbf{Z}_{oo}\mathcal{G}_{oo}-\mathcal{G}'_{oo})\mathbf{K}_{oo}=\mathcal{J}'_{oo}-\mathbf{Z}_{oc}\mathcal{J}_{co}-\mathbf{Z}_{oo}\mathcal{J}_{oo} . \quad (53)$$

Equation (53) is easily solved for $\mathbf{K}_{oo}$, from which the S matrix is obtained as

$$\mathbf{S}=(\mathbf{I}-i\mathbf{K}_{oo})^{-1}(\mathbf{I}+i\mathbf{K}_{oo}) . \tag{54}$$

The system of coupled-channel equations is integrated from $\rho_{\min}\approx 0$ to ρ_{as} for which the S matrix is a (ρ-independent) constant.

III. RESULTS AND DISCUSSION

A. Bound-state calculations

As a useful check of the method we have performed a number of bound-state calculations. Since our final aim is the photoionization cross sections we did not attempt to exceed the accuracy of other methods by pushing the bound-state calculation to complete convergence. The method for calculating bound states is based on locating the poles of $S_{a',a}(E)$ of Eq. (42). We use two (identical) artificial channels and a set of closed physical channels. Plots of the artificial and the closed-channel potentials for H^- are presented in Fig. 4. As shown there the artificial potentials do allow for good overlap between the bound- and artificial-channel wave functions.

The energy dependence, showing a pole, of a typical $S_{a'a}$ matrix element in the vicinity of the H^- ground-state energy, is shown in Fig. 5. In Table II we provide details of the 17-channel calculation (15 closed channels and 2 artificial channels) needed to locate the ground-state energy to sufficient accuracy. Table III presents a convergence study of the ground-state energies of H^- and He with the number of channels. We see that the energy eigenvalues converge monotonically from below, with the 17-channel value being $E_{H^-}=-0.527\,642$ a.u. and $E_{He}=-2.903\,611$ a.u. As shown in Table IV, these values are very close to Pekeris' values [46]. $E^{var}_{H^-}=-0.527\,751$ a.u. and $E^{var}_{He}=-2.903\,724$ a.u. Comparisons with other calculations are also given in Table IV. We can see that our ground-state energies are as accurate (sometimes even more so) as those obtained by other *ab initio* methods.

B. Photodetachment of H^-

The nuclear charge of the negative hydrogen ion is smaller than the number of electrons. As a result H^- has different properties from the other heliumlike systems: the electron-electron interaction is as strong as the nucleus-electron one, leading to strong correlational effects; the continuum states are governed by the long-range polarization of the core by the continuum electron. In addition, H^- has only one bound state.

Past studies of the H^- photodetachment, such as those based on the hyperspherical adiabatic approximation [29], suffer from substantial discrepancies between the length and acceleration forms, at least in the energy range of $\{0.03-0.22\}$ a.u. This discrepancy completely disappears, as we show below, when nonadiabatic effects are properly taken into account.

The convergence of the H^- photodetachment cross section (in the length form) with the number of continuum coupled channels is presented in Table V. In Table VI we present converged 36-channel (20 continuum channels, 15 bound channels, and one extra artificial channel) results for the H^- photodetachment cross sections for photoelectron energies between 0.01 and 0.70 Ry. Also included in Table VI are calculations based on the acceleration form which are seen to be in excellent agreement with the length-form calculations for k^2 ranging from 0.01 to 0.70 Ry. Comparisons with previous calculations [11,47,48,50–54], are also included in Table VI.

Our acceleration-form results can be compared with the perturbation-variation calculation by Stewart [51] and with the variational calculation of Geltman [50] performed with a 70-parameter Schwartz function for the bound state and an extensively correlated continuum state. We see that our results are superior since the acceleration-form calculations of Geltman [50] differ substantially from those of the length form. Possibly this failure is due to differences in the treatment of the short-range electron correlation between the bound and $^1P^o$ continuum states. In contrast, in the artificial-channel method the bound and scattering states are treated on an equal footing.

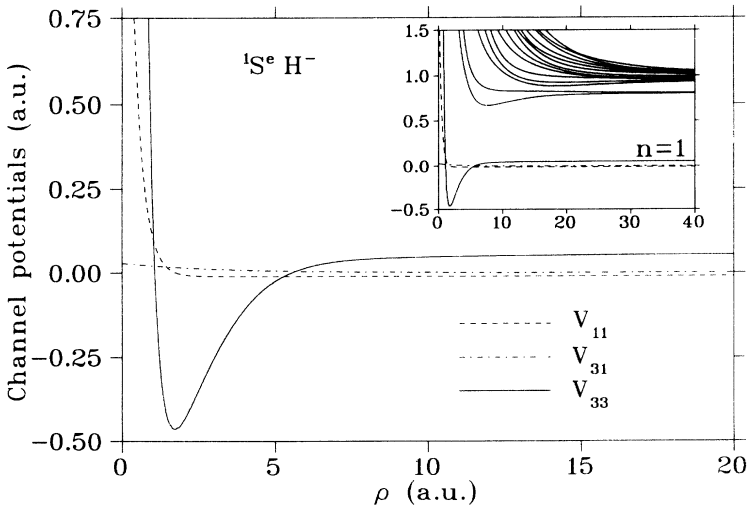

FIG. 4. Artificial and diagonal channel potentials for the H^- bound manifold.

TABLE II. Details of the ground-state energy level calculation for H^- and He. The numbers in brackets represent the power of ten. Energy is expressed in a.u.

Calculation number	Energy		$\mathrm{Im}(S_{a'a})/\cos\delta_a$	
	H^-	He	H^-	He
1	−0.527 651 00	−2.903 624 37	−0.618[+2]	−0.101[+2]
2	−0.527 651 00	−2.903 624 37	−0.509[+1]	−0.119[+1]
3	−0.527 642 04	−2.903 611 13	0.538[+5]	0.433[+4]
4	−0.527 642 05	−2.903 611 16	0.603[+9]	−0.124[+8]
5		−2.903 611 16		−0.336[+8]

Our length- and acceleration-form results are also compared in Table VI with the following calculations:

(i) The length-form results by Bell and Kingston [52] using the Schwartz function for the ground state and polarized-orbital functions for continuum state.

(ii) Ajmera and Chung [53] using the 33-parameter Hylleraas-type ground-state wave function with an asymptotic "tail function" and continuum wave function obtained by the simplified Kohn-Feshbach variational method.

(iii) Broad and Reinhardt [47] multichannel J-matrix calculation using 67 configurations of Slater-type orbitals for the bound state and 160 configurations of Laguerre-type functions approximating 36 scattering channels.

(iv) Wishart [48] using the close-coupling method with pseudostates and Hylleraas-type correlation terms.

(v) Daskhan and Ghosh [54] using the 70-parameter Schwartz ground-state function and continuum function obtained by a polarized-orbital method with accounting a distorted-target wave function.

(vi) Saha [11] using the multiconfigurational Hartree-Fock method including 32 configurations for the ground state and 36 configurations for continuum state.

In order to highlight the differences between the various calculations we have plotted in Fig. 6 both the length- and acceleration-form cross sections vs the photoelectron energy obtained by us and by the above-mentioned authors.

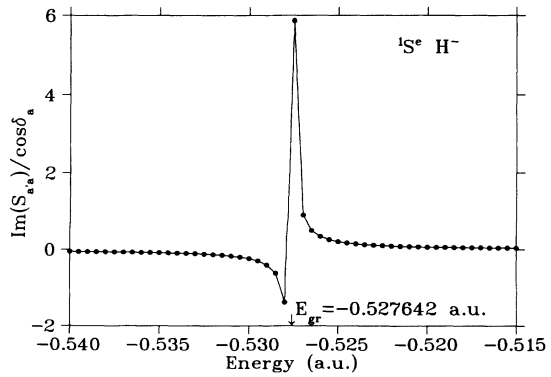

FIG. 5. Behavior of $\mathrm{Im}(S_{a'a})/\cos\delta_a$ as a function of energy in the vicinity of the H^- ground-state eigenvalue.

Analysis of Table VI and Fig. 6 shows that our length-form results are in very close agreement with the very extensive calculations of Saha [11], Stewart [51], and Wishart [48]. Our acceleration-form results are almost as accurate over the entire 0.025–0.075-a.u. range. Notice also the excellent agreement between our length- and acceleration-form cross sections which differ at most by 0.065×10^{-17} cm^2 (and usually by much less). The agreement between the two forms becomes even better with increasing k^2.

In Fig. 7 we have plotted our length and acceleration cross sections as a function of the incident photon wavelength from 4000 to 14 000 Å. Also included are the theoretical results of Refs. [11,48,50,51] and the relative experimental cross sections of Smith and Burch [55], normalized to the present length-form curve at 5280 Å (k^2=0.117 Ry). At 5280 Å our length- and acceleration-form results are, respectively, 3.081 and 3.049 in units of 10^{-17} cm^2, both well within the error bars of the experimental value of 3.28±0.3, determined by Geltman [50] from the absolute integrated measurements of Branscomb and Smith [56].

Our computed values compare very favorably with the length-form calculations for Stewart [51] (3.068 in the same units), Bell and Kingston [52] (3.08), Ajmera and Chung [53] (3.06), Broad and Reinhardt [47] (3.019), Wishart [48] (3.078), and Saha [11] (3.074). In the long-wavelength region the agreement between our results and the experimental ones is in fact better than that of all other calculations.

C. Photoionization of He

The photoionization of He serves as an important test case for different theories and computational schemes.

TABLE III. Convergence of the ground-state energy (in a.u.) and relevant width amplitude (the residue of the S-matrix pole) for H^- and He with the number of coupled channels.

Number of channels	Energy		Width amplitude	
	H^-	He	H^-	He
1+2	−0.536 499	−2.925 340	0.006 183 2	0.001 703 0
3+2	−0.528 460	−2.904 855	0.005 640 3	0.001 378 8
6+2	−0.528 122	−2.904 682	0.005 578 9	0.001 360 5
10+2	−0.527 749	−2.903 736	0.005 551 0	0.001 343 8
15+2	−0.527 642	−2.903 611	0.005 535 4	0.001 338 2

TABLE IV. Comparison of the present ground-state energy (in a.u.) of H^- and He with other theoretical calculations.

Method	H^-	He
ACM[a]	−0.527 642	−2.903 611
HSCC[b]		−2.903 594
HSA[c]	−0.527 746	−2.903 698
VAR[d]	−0.527 751	−2.903 724
MCHF[e]	−0.527 542	−2.902 909
CI[f]	−0.527 542	−2.903 23
RMM[g]	−0.524 03	−2.8961
CCM[h]	−0.527 75	−2.8934

[a]Present 17-channel artificial-channel method calculation.
[b]Hyperspherical 21-channel close-coupling calculation [17].
[c]Six-channel hyperspherical adiabatic calculation [35(a),37].
[d]Variational method calculation [46].
[e]Multiconfigurational Hartree-Fock calculation: using 32 configurations for H^- [11] and 10 configurations for He [12].
[f]Configuration interaction method calculation: using 130 configurations for H^- [13(b)] and He [13(a)].
[g]R-matrix method calculations: using 158 configurations for H^- [9] and 79 configurations for He [8(a)].
[h]Close-coupling method calculation with pseudostates and correlation terms: nine Hylleraas-type functions for H^- [48] and seven correlation functions for He [49].

Over the last few years, a large number of calculations of the photoionization of ground-state He using a variety of sophisticated techniques have been published [8(a),10,12,13(a),14(a),15,16,18,49]. Most of the recent computations of the photoionization cross sections agree with each other and with earlier calculations to better than 4%, a value nearing the precision of modern experiments [57], estimated to be better than 2% in the 0–120-eV range. Direct comparisons between theory and experiment are therefore possible.

In Fig. 8 we present the length- and acceleration-form photoionization cross sections of He, calculated using 26 channels (10 channels for scattering-state manifold, 15 channels for bound-state manifold, and one artificial channel). Our length- and acceleration-form cross sections coincide to better than two significant figures over the whole energy range considered. As in the H^- case, the agreement between the acceleration-form and length-form calculations further improves with increasing energy.

TABLE V. Convergence of H^- photodetachment cross section (in units of 10^{-17} cm^2) with the number of coupled channels of the "continuum manifold." The number of "bound manifold" channels used in the calculation is fixed at 15.

k^2	Number of channels for ^1P continuum state					
(Ry)	4	9	12	16	19	22
0.04	3.950	3.938	3.891	3.883	3.911	3.909
0.06	3.883	3.947	3.938	3.958	3.979	3.979
0.08	3.567	3.641	3.669	3.692	3.700	3.711
0.10	3.234	3.303	3.350	3.371	3.370	3.375
0.16	2.361	2.405	2.444	2.456	2.457	2.461
0.32	1.216	1.235	1.237	1.238	1.238	1.238
0.64	0.573	0.570	0.570	0.570	0.570	0.570

Both our length-form and acceleration-form results are in very good agreement with the high-precision measurements by Samson *et al.* [57]. In Fig. 8 we also plot other theoretical cross sections of the following authors: (i) Stewart and Webb [58] (length- and acceleration-form calculations using six-parameter Hylleraas-type ground-state function and Hartree-Fock continuum wave function); (ii) Burke and McVicar [59] (close-coupling $1s$-$2s$-$2p$ length-form calculation using the Hart-Herzberg 20 parameter ground-state wave function); (iii) Bell and Kingston [60] (length-form calculation using 20 parameter Hylleraas-type bound-state function and polarized-orbital continuum wave function). We forego here additional literature surveys of He photoionization calculations, since an extensive analysis, including a dis-

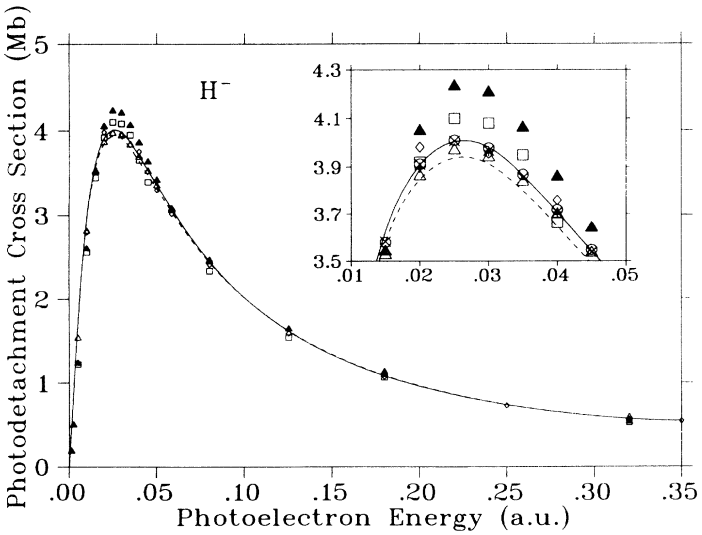

FIG. 6. $H^-(^1S)+h\nu\rightarrow H(1s)(^2S)+e^-(kp)$ photodetachment cross section vs photoelectron energy ——, present length-form results; — — —, present acceleration-form results; length-form results of: o, Stewart [51]; ▲, Bell and Kingston [52]; △, Ajmera and Chung [53]; ◇, Broad and Reinhardt [47]; +, Wishart [48]; □, Daskhan and Ghosh [54]; ×, Saha [11].

TABLE VI. Comparison of the present photodetachment cross section of H^- (in units of 10^{-17} cm^2) as a function of photoelectron energy (in Ry) with other theoretical calculations. *L* denotes the length form and *A* the acceleration form.

k^2	Present		St[a]		G[b]	BK[c]	AC[d]	BR[e]	W[f]	DG[g]	S[h]
(Ry)	*L*	*A*	*L*	*A*	*L*	*L*	*L*	*L*	*L*	*L*	*L*
0.01	1.645	1.641	1.565	1.429	1.197	1.234	1.531		1.553	1.221	1.55
0.02	2.971	2.945	2.862	2.546	2.509	2.600	2.810	2.798	2.846	2.559	2.868
0.03	3.601	3.556	3.580	3.113	3.411	3.540	3.525			3.461	3.583
0.04	3.910	3.851	3.912	3.363		4.048	3.863	3.982	3.898	3.920	3.911
0.05	4.006	3.940	4.010		4.090	4.231	3.968			4.100	4.007
0.06	3.979	3.915	3.978	3.377	4.079	4.205	3.940	3.956	3.965	4.080	3.968
0.07	3.876	3.811	3.870		3.952	4.060	3.838			3.950	3.857
0.08	3.706	3.645	3.717	3.152	3.767	3.859	3.695	3.759	3.708	3.663	3.707
0.09	3.534	3.480	3.548	3.014	3.560	3.640	3.533			3.409	3.538
0.10	3.375	3.327	3.373	2.874	3.351	3.432	3.364	3.313	3.368		3.364
0.117	3.081	3.049	3.068			3.08	3.06	3.019	3.078		3.074
0.16	2.450	2.436	2.450		2.358	2.447	2.463	2.41		2.335	2.443
0.25	1.616	1.621	1.595	1.467	1.558	1.643		1.591		1.541	1.599
0.36	1.082	1.088	1.058		1.050	1.129	1.094	1.072		1.064	1.065
0.50	0.737	0.739	0.716	0.694				0.729	0.728		0.722
0.64	0.569	0.570	0.547		0.522	0.531	0.584	0.560		0.523	0.553
0.70	0.547	0.547	0.523	0.509				0.543	0.539		0.525

[a]St, Stewart [51].
[b]G, Geltman [50].
[c]BK, Bel and Kingston [52].
[d]AC, Ajmera and Chung [53].
[e]BR, Broad and Reinhardt [47].
[f]W, Wishart [48].
[g]DG, Daskhan and Ghosh [54].
[h]S, Saha [11].

cussion of the validity of the adiabatic approximation has recently been published [17,18].

IV. CONCLUSIONS

In this paper we have presented a method based on the artificial channel method for calculating bound-state energies and photoionization processes in two-electron systems. The method treats the bound and continuum manifolds on an equal footing. The uniformity in accuracy thus achieved results in excellent agreement between the length and acceleration forms.

We have studied the photodetachment of the H^- ion

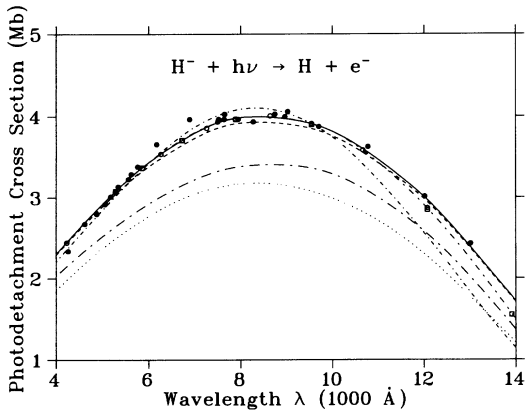

FIG. 7. H^- $(^1S)+h\nu\rightarrow H$ $(1s)(^2S)+e^-(kp)$ photodetachment cross section vs photon wavelength. ●, experimental results of Smith and Burch [55]; ——, present length-form results; — — —, present acceleration-form results; –·–, Stewart perturbation-variation length-form calculation [51]; —·—, Stewart acceleration-form calculation [51]; —·—·—·, Geltman variational length-form calculation [50] using the 70-parameter Schwartz bound state and fully correlated continuum state function; · · · ·, Geltman variational acceleration-form calculation [50]; ○, length-form multiconfigurational Hartree-Fock calculation of Saha [11]; □, length-form close-coupling pseudostate calculation with Hylleraas-type correlation terms by Wishart [48].

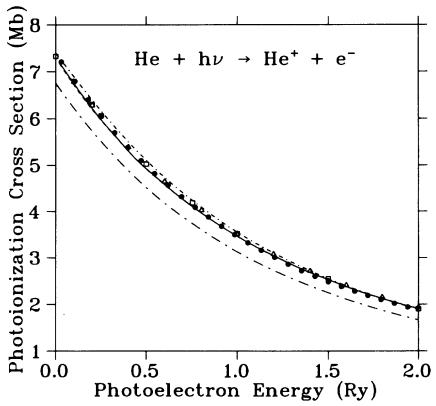

FIG. 8. He $(^1S)+h\nu\rightarrow He^+$ $(1s)(^2S)+e^-(kp)$ photoionization cross section vs photoelectron energy. ●, experimental results of Samson *et al.* [57]; ——, present length-form results; — — —, present acceleration-form results; —·—·, Stewart and Webb length-form calculation [58] using the six parameter Hylleraas-type ground-state function and the Hartree-Fock continuum wave function; —·—, Stewart and Webb acceleration-form calculation [58]; △, Burke and McVicar 1*s*-2*s*-2*p* close-coupling length-form calculation [59]; □, Bell and Kingston length-form calculation [60] using the 20-parameter Hylleraas-type ground-state wave function and the polarized-orbital continuum wave function.

and the photoionization of ground-state He. The results obtained are in excellent agreement with experiment throughout the range of energies considered. There is also a very close agreement with theoretical results obtained with some well-established methods.

The method can be used for describing the recent experimental observations [1–6] of the high-lying photoionization spectra of two-electron atoms. It can also be applied with minor modifications (see Ref. [19]) to the calculation of the positions and widths of the doubly excited (autoionizing) states of two-electron systems. The methodology presented here is not limited to atomic systems. Any two-electron molecular system can be solved (within the Born-Oppenheimer approximation) with this method. Extensions to the strong field domain [61] and for multiphoton processes [62], will be published soon.

ACKNOWLEDGMENT

We are grateful to Professor J. A. R. Samson for providing us with his experimental data for the He photoionization prior to publication.

[1] M. Zubek, G. C. King, P. M. Rutter, and F. H. Read, J. Phys. B **22**, 3411 (1989).

[2] M. Domke, C. Xue, A. Puschmann, T. Mandel, E. Hudson, D. A. Shirley, G. Kaindl, C. H. Greene, H. R. Sadeghpour, and H. Petersen, Phys. Rev. Lett. **66**, 1306 (1991).

[3] P. G. Harris, H. C. Bryant, A. H. Mohadheghi, R. A. Reeder, H. Sharifan, C. Y. Tang, H. Tootoonchi, J. B. Donahue, C. R. Quick, D. C. Rislove, W. W. Smith, and J. E. Stewart, Phys. Rev. Lett. **65**, 309 (1990); P. G. Harris, H. C. Bryant, A. H. Mohadheghi, R. A. Reeder, C. Y. Tang, J. B. Donahue, and C. R. Quick, Phys. Rev. A **42**, 6443 (1990).

[4] M. Halka, H. C. Bryant, E. P. Mackerrow, W. Miller, A. H. Mohadheghi, C. Y. Tang, S. Cohen, J. B. Donahue, A. Hsu, C. R. Quick, J. Tiee, and K. Rozsa, Phys. Rev. A **44**, 6127 (1991).

[5] P. G. Harris, H. C. Bryant, A. H. Mohadheghi, C. Tang, J. B. Donahue, C. R. Quick, R. A. Reeder, S. Cohen, W. W. Smith, J. E. Stewart, and C. Johnstone, Phys. Rev. A **41**, 5968 (1990).

[6] M. Halka, P. G. Harris, A. H. Mohadheghi, R. A. Reeder, C. Y. Tang, H. C. Bryant, J. B. Donahue, and C. R. Quick, Phys. Rev. A **48**, 419 (1993).

[7] S. M. Burkov, N. A. Letyaev, S. I. Strakhova, and T. M. Zajac, J. Phys. B **21**, 1195 (1988).

[8] M. A. Hayes and M. P. Scott, J. Phys. B **21**, 1499 (1988); (a) P. Hamacher and J. Hinze, *ibid.* **22**, 3397 (1989); S. M. Burkov, N. A. Letyaev, and S. I. Strakhova, Phys. Lett. A **150**, 31 (1990).

[9] H. R. Sadeghpour, C. H. Greene, and M. Cavagnero, Phys. Rev. A **45**, 1587 (1992).

[10] S. Solomonson, S. L. Carter, and H. P. Kelly, Phys. Rev. A **39**, 5111 (1989).

[11] H. P. Saha, Phys. Rev. A **38**, 4546 (1988).

[12] C. F. Fischer and M. Idrees, J. Phys. B **23**, 679 (1990).

[13] (a) I. Sánchez and F. Martín, J. Phys. B **23**, 4263 (1990); Phys. Rev. A **44**, 13, 7318 (1991); **45**, 4468 (1992); **48**, 1243 (1993); F. Martín, *ibid.* **48**, 331 (1993); (b) M. Cortés and F. Martín, *ibid.* **48**, 1227 (1993).

[14] T. N. Chang and R.-Q. Wang, Phys. Rev. A **43**, 1218 (1991); T. N. Chang and X. Tang, *ibid.* **44**, 232 (1991); (a) T. N. Chang and M. Zhen, *ibid.* **47**, 4849 (1993).

[15] R. Moccia and P. Spizzo, Phys. Rev. A **43**, 2199 (1991).

[16] D. L. Lynch and B. I. Schneider, Phys. Rev. A **45**, 4494 (1992).

[17] J. Z. Tang, S. Watanabe, and M. Matsuzawa, Phys. Rev. A **46**, 2427 (1992).

[18] J. Z. Tang, S.Watanabe, and M. Matsuzawa, Phys. Rev. A **46**, 3758 (1992); J. Z. Tang, S. Watanabe, M. Matsuzawa, and C. D. Lin, Phys. Rev. Lett. **69**, 1633 (1992).

[19] M. Shapiro, J. Chem. Phys. **56**, 2582 (1972).

[20] M. Shapiro and R. Bersohn, Annu. Rev. Phys. Chem. **33**, 409 (1982); G. G. Balint-Kurti and M. Shapiro, in *Photodissociation and Photoionization,* edited by K. P. Lawly (Wiley, New York, 1985), p. 403; Adv. Chem. Phys. **60**, 403 (1985).

[21] J. L. Krause and M. Shapiro, J. Chem. Phys. **90**, 6401 (1989).

[22] B. R. Johnson, J. Comput. Phys. **13**, 445 (1973).

[23] D. E. Manolopoulus, J. Chem. Phys. **85**, 6425 (1986).

[24] L. M. Delves, Nucl. Phys. **9**, 391 (1959); **20**, 275 (1960).

[25] J. Macek, J. Phys. B **1**, 831 (1968).

[26] U. Fano, Rep. Prog. Phys. **46**, 97 (1983); C. D. Lin, Adv. At. Mol. Phys. **22**, 77 (1986).

[27] $\mathcal{S}_\rho^5 \equiv \{\alpha, \hat{\mathbf{r}}_1, \hat{\mathbf{r}}_2\}$, where $\alpha = \tan^{-1}(r_2/r_1)$ is a hyperangle and $\hat{\mathbf{r}}_i = (\theta_i, \phi_i)$, $i = 1,2$, are usual spherical angles of the radius vectors $\mathbf{r}_i \equiv (\mathbf{r}_i, \theta_i, \phi_i)$.

[28] M. G. J. Fink and P. Zoller, J. Phys. B **18**, L373 (1985).

[29] C. H. Park, A. F. Starace, J. Tan, and C. D. Lin, Phys. Rev. A **33**, 1000 (1986).

[30] C. R. Liu and A. F. Starace, Phys. Rev. Lett. **62**, 407 (1989); Phys. Rev. A **40**, 4926 (1989); **42**, 2684 (1990).

[31] C. H. Greene, J. Phys. B **13**, L39 (1980); H. R. Sadeghpour and C. H. Greene, Phys. Rev. Lett. **65**, 313 (1991); H. R. Sadeghpour, Phys. Rev. A **43**, 5821 (1991).

[32] C. R. Liu, N. Y. Du, and A. F. Starace, Phys. Rev. A **43**, 5891 (1991).

[33] K. Moribayashi, K.-I. Hino, and M. Matsuzawa, Phys. Rev. A **44**, 7234 (1991).

[34] A. G. Abrashkevich, S. I. Vinitsky, M. S. Kaschiev, and I. V. Puzynin, Yad. Fiz. **48**, 945 (1988) [Sov. J. Nucl. Phys. **48**, 602 (1988)].

[35] (a) A. G. Abrashkevich, D. G. Abrashkevich, M. S. Kaschiev, I. V. Puzynin, and S. I. Vinitsky, J. Phys. B **22**, 3957 (1989); A. G. Abrashkevich, D. G. Abrashkevich, I. V. Puzynin, and S. I. Vinitsky, *ibid.* **24**, 1615 (1991); A. G. Abrashkevich, D. G. Abrashkevich, I. V. Khimich, I. V. Puzynin, and S. I. Vinitsky, *ibid.* **24**, 2807 (1991).

[36] A. G. Abrashkevich, D. G. Abrashkevich, M. S. Kaschiev, I. V. Puzynin, and S. I. Vinitsky, Phys. Rev. A **45**, 5274 (1992).

[37] A. G. Abrashkevich, D. G. Abrashkevich, M. I. Gaysak, V. I. Lendyel, I. V. Puzynin, and S. I. Vinitsky, Phys. Lett. A **152**, 467 (1991).

[38] D. M. Hood and A. Kuppermann, in *Theory of Chemical Reaction Dynamics,* edited by D. C. Clary (Reidel, Boston, 1986), pp. 193–214.

[39] K. J. Bathe, *Finite Element Procedures in Engineering Analysis* (Prentice-Hall, Englewood Cliffs, NJ, 1982).
[40] F. T. Smith, Phys. Rev. **179**, 111 (1969).
[41] B. L. Christensen-Dalsgaard, Phys. Rev. A **29**, 470 (1984).
[42] J. C. Light and R. B. Walker, J. Chem. Phys. **65**, 4272 (1976); B. Lepetit, J. M. Launay, and M. LeDourneuf, Chem. Phys. **106**, 103 (1986).
[43] The only limitation on our choice of V_0 and a is imposed by the requirement that the artificial wave function F^a indeed serves as an effective source term. This requirement is satisfied by ensuring non-negligible spatial overlap between the artifical wave function and the bound manifold coupled to it.
[44] M. Shapiro and G. G. Balint-Kurti, J. Chem. Phys. **71**, 1461 (1978).
[45] G. G. Balint-Kurti, R. E. Moss, I. A. Sadler, and M. Shapiro, Phys. Rev. A **41**, 4913 (1990).
[46] C. L. Pekeris, Phys. Rev. **126**, 1470 (1962).
[47] J. T. Broad and W. P. Reinhardt, Phys. Rev. A **14**, 2159 (1976).
[48] A. W. Wishart, J. Phys. B **12**, 3511 (1979).
[49] J. A. Fernley, K. T. Taylor, and M. J. Seaton, J. Phys. B **20**, 6457 (1987).
[50] S. Geltman, Astrophys. J. **136**, 935 (1962).
[51] A. L. Stewart, J. Phys. B **11**, 3851 (1978).
[52] K. L. Bell and A. E. Kingston, Proc. Phys. Soc. London **90**, 895 (1967).
[53] M. P. Ajmera and K. T. Chung, Phys. Rev. A **12**, 475 (1975).
[54] M. Daskhan and A. S. Ghosh, Phys. Rev. A **28**, 2767 (1983).
[55] S. J. Smith and D. S. Burch, Phys. Rev. Lett. **2**, 165 (1959); Phys. Rev. **116**, 1125 (1959).
[56] L. M. Branscomb and S. J. Smith, Phys. Rev. **98**, 1028 (1955).
[57] J. A. R. Samson, Z. X. He, L. Yin, and G. N. Haddad, J. Phys. B **27**, 887 (1994).
[58] A. L. Stewart and T. G. Webb, Proc. Phys. Soc. London **82**, 532 (1963).
[59] P. G. Burke and D. D. McVicar, Proc. Phys. Soc. London **86**, 989 (1965).
[60] K. L. Bell and A. E. Kingston, Proc. Phys. Soc. London **90**, 31 (1967).
[61] A. G. Abrashkevich and M. Shapiro (unpublished).
[62] R. Blank and M. Shapiro (unpublished).